Journal of Catalysis **205,** 318–331 (2002)
doi:10.1006/jcat.2001.3424, available online at http://www.idealibrary.com on IDEAL®

Effect of ZrO_2 Loading on the Structure, Acidity, and Catalytic Activity of the SO_4^{2-}/ZrO_2/MCM-41 Acid Catalyst

Q.-H. Xia,[1] K. Hidajat, and S. Kawi

Department of Chemical & Environmental Engineering, National University of Singapore, Singapore 119260

Received June 22, 2001; revised September 3, 2001; accepted September 8, 2001; published online January 3, 2002

The regular hexagonal structure of siliceous MCM-41 with a uniform mesopore size is still maintained after 48.5 wt% ZrO_2 loading. Under high loadings ($\geq$26.7%) of ZrO_2, a very small amount of ZrO_2 clusters (present as tetragonal ZrO_2 phase) might be formed inside or outside the MCM-41 structure. The hydrophobicity of the SO_4^{2-}/ZrO_2/MCM-41 catalysts is stepwise enhanced by increasing the ZrO_2 loading. The covalent S=O band 1378-cm^{-1} for the SO_4^{2-}/ZrO_2 catalyst shifts to 1363 cm^{-1} for SO_4^{2-}/ZrO_2/MCM-41 materials. Under identical ZrO_2 loading, SO_4^{2-}/ZrO_2/MCM-41 has stronger Brønsted and Lewis acidities than PMSZM/ZrO_2 (physical mixture of SO_4^{2-}/ZrO_2 and MCM-41). The SO_4^{2-}/ZrO_2/MCM-41 catalysts show high activity with a selective conversion of >95 mol% Bu^{t}OH to MTBE at low temperatures below 160°C, further showing the excellent on-stream stability of these catalysts for this reaction. The rather poor activity of PMSZM/ZrO_2 catalysts has been ascribed to their weak acidity.

Key Words: **SO_4^{2-}/ZrO_2/MCM-41; solid acid; acidity; gas-phase synthesis of MTBE.**

1. INTRODUCTION

Zirconia modified with sulfate anions can form a highly acidic catalyst which was previously considered to be a solid superacid, characterized by Hammett indicators (1–3), 10^4 times stronger than 100% sulfuric acid. Sulfated zirconia (SO_4^{2-}/ZrO_2) possesses a unique acid catalytic activity, and its low-temperature activity for hydrocarbon isomerization is well documented, especially for the isomerization of *n*-butane to iso-butane, a hydrocarbon used in the production of oxygenates and alkylates. However, the acid strength of sulfated zirconia is still open to debate. On one hand, sulfated zirconia is considered to have superacidic acid sites or very strong acid sites (4–7). On the other hand, the earlier use of Hammett indicators making sulfated zirconia a strong solid superacid having Ho of −13.5 to −16.0 is considered to be unreliable (8). Some reports have concluded that sulfated zirconia is not a superacid and that its acidity is similar to that of HY but less than that of HZSM-5 (9–12). Recently, however, based on the kinetics of the catalytic conversion of iso-butane, Fraenkel (13) proposed that sulfated zirconia may be a very strong solid superacid. Another study reported that the acid strength of sulfated zirconia is higher than those of $Cs_{2.5}H_{0.5}PW_{12}O_{40}$ heteropolyacid and zeolites such as HY, HZSM-5, and HMOR based on the activation energy of Ar desorption from these solid acids determined by TPD at lower temperatures (14). Recently, Sommer *et al*. (15, 16) also reported that the acidity of sulfated zirconia is greater than that of HZSM-5, based on the H/D exchange of methane, and suggested that sulfated zirconia may possess very strong acid sites.

In recent years, sulfated zirconia and related materials have attracted increasing attention because these catalysts were found to be well suited for catalyzing reactions of industrial importance, such as hydrocarbon isomerization, etherification reactions, etc. (1–3, 17–22). However the nonuniform pore size and relatively small surface area of these acidic catalysts may limit their potential application for catalyzing bulky molecules, such as those encountered in the synthesis of pharmaceuticals and fine chemicals.

The use of M41s and other mesoporous materials (23–26), which have very uniform mesopores and very high surface areas, as catalyst supports for SO_4^{2-}/ZrO_2 should greatly expand the catalytic properties and capabilities of SO_4^{2-}/ZrO_2 for some applications. This is because such mesoporous materials, which have a relatively small diffusion hindrance, can aid the diffusion of bulky organic molecules in and out of their mesopores quite easily (23). Although many sulfated zirconia-based catalysts have been developed using SiO_2, Al_2O_3, and microporous zeolites as supports, there are still many limitations in their applications because of diffusion problems. Although direct preparations of mesoporous sulfated zirconia and zirconium oxide–sulfate have been recently reported (27, 28), the resulting materials had relatively small surface areas, comparable to that of conventional SO_4^{2-}/ZrO_2. Therefore a successful development of silica-based M41s sulfated zirconia materials will be of industrial significance.

Due to high octane number, MTBE (methyl-*tert*-butyl ether) is the most widely used quality-improving additive

[1] To whom correspondence should be addressed.

0021-9517/02 $35.00

for unleaded gasolines. It easily mixes with gasoline, has excellent antiknocking behavior, and reduces the emission of pollutants. However, it should be mentioned that MTBE is presently being scrutinized for potential environmental damage to groundwater and to the atmosphere (29–33). MTBE as a gasoline oxygenate has influenced environmental public policy in the United States. Legislation is being introduced to ban MTBE (34–36). In the near future, the use of MTBE will be reduced and could be replaced by ethanol or other oxygenates that are less harmful to the environment (37).

MTBE is industrially synthesized from methanol and isobutene over a sulfonated ion-exchange resin such as Amberlyst-15 (38). It is also produced through reacting *tert*-butanol with methanol over an acidic catalyst yielding water as a co-product. Since the Amberlyst-15 catalyst for this synthesis suffers severe drawbacks, such as not being stable thermally and chemically (39), many acidic catalysts such as traditional microporous zeolites and heteropoly acids (40–43) have been developed to catalyze the occurrence of these reactions. Quiroga *et al*. (44) studied the synthesis of MTBE from methanol and isobutylene in a gas–solid heterogeneous system over SO_4^{2-}/ZrO_2 catalyst and found that the catalyst acidity was a direct function of the amount of sulfur loading. Due to its acid-catalyzed characteristics, this reaction has been frequently used as a probing reaction for ascertaining the acidity of heterogeneous catalysts.

Recently, we reported the successful synthesis of a new mesoporous acidic catalyst, SO_4^{2-}/ZrO_2/MCM-41, which was found to be more active than the conventional SO_4^{2-}/ZrO_2 catalyst (26). In the present work, the research is mainly focused on the effect of ZrO_2 loading on the structure, and the hydrophobicity, acidity, and catalytic activity of the SO_4^{2-}/ZrO_2/MCM-41 acid catalyst. To evaluate the acidity and catalytic activity of these catalysts, the gas-phase synthesis of MTBE from MeOH and Bu^tOH is carried out in a continuous fixed-bed reactor. We have observed that when ZrO_2 loading on MCM-41 is as low as 5.5% (weight percent), the resulting SO_4^{2-}/ZrO_2/MCM-41 catalyst still has a very high catalytic activity for the aforementioned synthesis of MTBE; however, the acidity of the catalyst is rather weak. As a comparison, the structure, acidity, and catalytic activity of the physical mixture of SO_4^{2-}/ZrO_2 and MCM-41 (PMSZM/ZrO_2) with the same composition have been studied.

2. EXPERIMENTAL

2.1. Synthesis of Catalysts

As the support, fluorinated siliceous MCM-41, which has a highly hydrophobic surface, was synthesized in a fluoride medium according to the synthesis procedure in the literature (45, 46). $Zr(OH)_4$ was supported on the surface of MCM-41 through chemical liquid deposition and hydrolysis of $Zr(OPr^n)_4$ rather than traditional anhydrous $ZrCl_4$. This is because when $ZrCl_4$ was used as a precursor in the preparation of $Zr(OH)_4$/MCM-41, the mesoporous structure of MCM-41 collapsed in the basic medium required for the hydrolysis of $ZrCl_4$ (26). Predried siliceous MCM-41 (Si-MCM-41) powder, with a 1311-m^2/g BET surface area and a 31.4-Å pore diameter, was dispersed into a mixed solution of zirconium *n*-propoxide and *n*-hexane under vigorous stirring. After evaporating the solvent, the solid was transferred onto a porous ceramic plate in a glass container to adsorb water vapor from the NaCl–saturated water solution at the bottom for complete hydrolysis at room temperature overnight. Pure $Zr(OH)_4$ was also prepared through the hydrolysis of anhydrous $ZrCl_4$ in an ammonia solution with a pH of 9–10 (17). After drying both samples at 96°C overnight, the resulting solids were immersed in 1.0 N sulfuric acid solution at room temperature for 30 min. The sulfated $Zr(OH)_4$/MCM-41 and $Zr(OH)_4$ were then filtered off, dried at 96°C overnight, and calcined at 600°C in air for 3 h to form SO_4^{2-}/ZrO_2/MCM-41 and SO_4^{2-}/ZrO_2 acid catalysts. The content of ZrO_2 in SO_4^{2-}/ZrO_2/MCM-41 catalysts was analyzed by ICP to be 48.5, 41.0, 26.7, 13.3, and 5.5 wt%. The physical mixture of SO_4^{2-}/ZrO_2 and MCM-41 was prepared through mechanically grinding SO_4^{2-}/ZrO_2 and MCM-41, followed by calcination at 550°C in air for 3 h. The resulting sample was designated as PMSZM/*x* %ZrO_2, where *x* % is the respective ZrO_2 content of 48.5, 41.0, 26.7, 13.4, and 5.4 wt%.

2.2. Characterizations of Catalysts

The XRD patterns of powder samples, which reflect the integrity and uniformity of mesoporous structures as well as the crystalline phase of ZrO_2 on the surface of MCM-41, were recorded by a Shimadzu XRD-6000 diffractometer using Ni-filtered Cu$K\alpha$ radiation operating at 40 kV and 30 mA. The 2θ range was from 1.5 to 70°. Autosorb-1 was used to measure the N_2 adsorption–desorption isotherms of the samples. Prior to the measurements, the samples were outgassed at 300°C overnight. The BET-specific surface area was calculated using the BET equation in the range of relative pressures between 0.05 and 0.25. The BJH method was used to calculate the pore volume and pore size distribution of the samples.

The weight–loss curves (TGA) of SO_4^{2-}/ZrO_2 and SO_4^{2-}/ZrO_2/MCM-41 catalysts were recorded on a Shimadzu DTG-50 thermogravimetric analyzer with a heating rate of 20°C/min from room temperature to 1000°C in an air flow of 50 cm^3/min. The *in situ* FTIR spectra of the S=O vibrational band, hydroxyl groups, and pyridine chemisorption were recorded using a Shimadzu FTIR-8700 spectrophotometer having a resolution of 4 cm^{-1} and connected to a PFEIFFER vacuum system, respectively. Before scanning the IR spectra of the S=O vibration and hydroxyl groups,

a self-supporting wafer (15 mg, with a pressure of 5 ton cm^{-2}) of the catalyst was evacuated at 300–400°C for 5 h in an *in situ* cell under vacuum at 10^{-6} mbar. The relative coverage of surface hydroxyl groups of the prepared SO_4^{2-}/ZrO_2/MCM-41 catalysts was evaluated by comparing the integrated area of the hydroxyl bands (3000–3750 cm^{-1}) of the solid product to that of the MCM-41 support. Pyridine adsorption *in situ* IR spectra were measured to determine the presence of Brønsted and Lewis acid sites over the catalysts. This was done by first pretreating a self-supporting wafer (15 mg) of the catalyst at 400°C for 3 h under vacuum at 10^{-6} mbar before adsorbing an excess of pure pyridine at room temperature, followed by evacuation at 200°C for 30 min. Brønsted and Lewis acidities were quantified into the integrated areas of the absorbance peaks at 1540 and at 1445 cm^{-1}, respectively. Scanning electron microscopy–energy dispersive X-ray (SEM–EDX) analysis was conducted on a JEOL JSM-5600LV scanning electron microscope using a silicon detector operating at an accelerating voltage of 15 kV and a beam current of 1.0 nA under vacuum at 10^{-6}–10^{-7} mbar. The element used for optimization was copper, and all quantitative results below 2 sigma were set to zero.

2.3. Catalytic Tests

For the gas–solid phase synthesis of MTBE from MeOH and Bu^tOH in a continuous fixed-bed reactor, 0.20 g of the catalyst (40–60 mesh pellets) was predehydrated at 300°C for 2 h in a flow of helium before a mixture of MeOH and Bu^tOH, with a molar ratio of 10 : 1, was pumped into the reactor ($\frac{1}{4}$ in. o.d.) and heated at given temperatures. During the reactions, a 13-ml/min helium flow was used as carrier and dilute gas, and the weight hourly space velocity (WHSV) was kept at 10 h^{-1}. The products were analyzed on stream by a Shimadzu GC-17A gas chromatograph equipped with a FID and an OV-1 capillary column. The molar conversion of Bu^tOH was calculated based on the selective conversion of Bu^tOH to MTBE, regardless of excessive MeOH.

3. RESULTS AND DISCUSSION

3.1. The Structure of SO_4^{2-}/ZrO_2/MCM-41 and PMSZM/ZrO_2 Materials

Figure 1 illustrates the effect of ZrO_2 loading on the XRD patterns of the SO_4^{2-}/ZrO_2/MCM-41 samples. Four distinct and intense diffraction peaks below 10° can be observed for the Si-MCM-41 support and the SO_4^{2-}/5.5%ZrO_2/MCM-41 sample; however, for the SO_4^{2-}/ZrO_2/MCM-41 samples loaded with more than 13.3% of ZrO_2, the [210] peak becomes obscure. Particularly, when the ZrO_2 loading is increased to 48.5 wt%, three clear diffraction peaks are still observed. The three- or four-peak XRD pattern in the small angle is usually used to characterize the long-range ordered

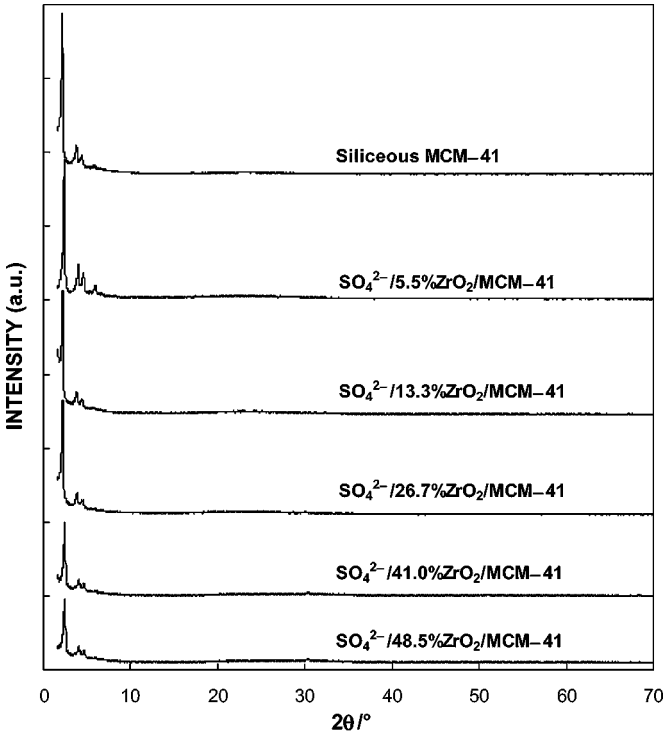

FIG. 1. The effect of ZrO_2 loading on the XRD patterns of SO_4^{2-}/ZrO_2/MCM-41 samples.

hexagonal mesostructures (23). The XRD results show that the MCM-41 support is still well maintained even after it has gone through the processes of chemical liquid deposition of ZrO_2, impregnation of sulfuric acid, and high-temperature calcinations.

However, the ZrO_2 amount has a striking effect on the intensity of the main XRD reflection [100] peak of the siliceous MCM-41 support, and this peak weakens proportionally to the increase of ZrO_2 loading. Figure 2 shows that, for SO_4^{2-}/ZrO_2 calcined at 600°C, three intense diffraction peaks at ca. 30, 50, and 60° and several small peaks at ca. 35 and 62° can be observed. These diffraction peaks can be indexed into the presence of the tetragonal ZrO_2 crystalline phase, rather than the monoclinic ZrO_2 phase, showing that the introduction of SO_4^{2-} anions can stabilize the metastable tetragonal ZrO_2 phase, which is considered to be an ideal crystalline phase for the SO_4^{2-}/ZrO_2 acid catalyst (2, 4, 6). Interestingly, when the XRD patterns in Fig. 1, in the range from 20 to 70°, are magnified ×5, three diffraction peaks at ca. 30, 50, and 60° can be observed for SO_4^{2-}/ZrO_2/MCM-41 samples with ZrO_2 loadings higher than 26.7 wt%. However, when the ZrO_2 loading is reduced to 13.3 and 5.5 wt%, the crystalline ZrO_2 phase cannot be detected. This suggests that, under increased ZrO_2 loading (≥26.7%) a very small amount of ZrO_2 clusters (present as a tetragonal ZrO_2 phase) might be formed inside or outside the MCM-41 structure, and the intensity of the tetragonal ZrO_2 phase

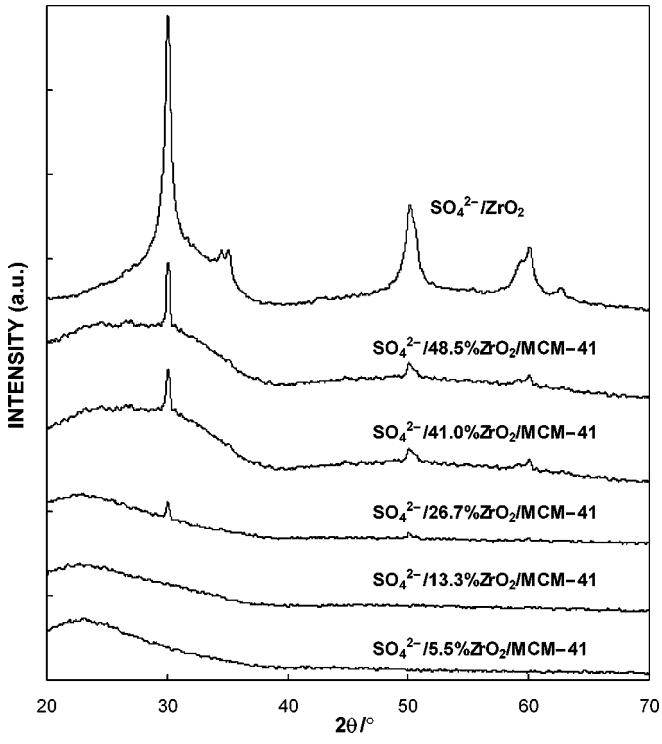

FIG. 2. The effect of ZrO_2 loading on the crystalline phase of ZrO_2 in SO_4^{2-}/ZrO_2/MCM-41 samples.

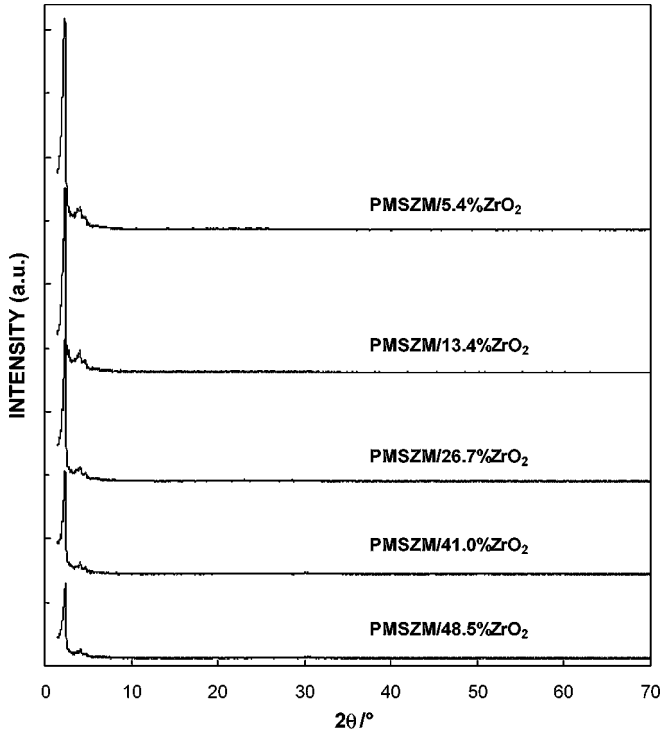

FIG. 3. The effect of ZrO_2 amount on the XRD patterns of PMSZM/ZrO_2 samples.

gradually increases with increased ZrO_2 loading. However, when ZrO_2 loading on MCM-41 is as high as 48.5 wt%, the XRD peak at $2\theta = 30^\circ$ appears even narrower than the corresponding peak of SO_4^{2-}/ZrO_2, suggesting that it might be a quite well crystallized species rather than well-dispersed and thus ill-defined zirconia aggregates.

The effect of the ZrO_2 amount on the XRD patterns in a physical mixture of SO_4^{2-}/ZrO_2 and MCM-41 is also investigated. The XRD patterns (in Fig. 3) in PMSZM/ZrO_2 samples having varying ZrO_2 amounts exhibit similar changes to those of SO_4^{2-}/ZrO_2/MCM-41 samples with varying amounts of ZrO_2 (in Fig. 1). However, as shown in Fig. 4, once the XRD patterns from 20 to 70° are magnified ×5, strong diffraction peaks at ca. 30, 50, and 60° similar to those of SO_4^{2-}/ZrO_2 can be observed for all PMSZM/ZrO_2 samples with ZrO_2 amounts of 13.4–48.5 wt%, and the intensities of these peaks decrease with decreasing ZrO_2 amounts. When the ZrO_2 amount is reduced to 5.4 wt%, a small diffraction peak at ca. 30° is still observable and this is remarkably different from the observation made in Fig. 2. It is conceivable that due to low dispersion through mechanical grinding, the tetragonal ZrO_2 crystalline phase is still well kept in the PMSZM/ZrO_2 samples.

BET analyses in Table 1 show that for the SO_4^{2-}/ZrO_2/MCM-41 samples, the BET surface area and pore volume reduce gradually with the increase of ZrO_2 loading; however, they are still much larger than those of the

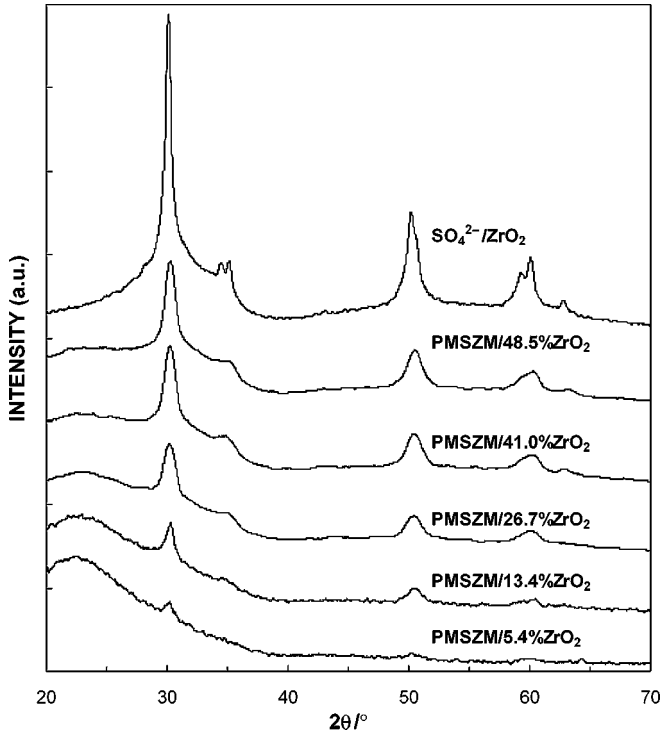

FIG. 4. The effect of ZrO_2 amount on the crystalline phase of ZrO_2 in PMSZM/ZrO_2 samples.

TABLE 1

BET Data of Si-MCM-41, SO_4^{2-}/ZrO_2, SO_4^{2-}/ZrO_2/MCM-41, and PMSZM/ZrO_2 Samples

Sample	BET surface area (m^2/g)	Pore volume (cm^3/g)	Pore diameter (Å)
Siliceous MCM-41	1311.0	1.03	31.4
SO_4^{2-}/5.5%ZrO_2/MCM-41	979.0	0.79	29.5
SO_4^{2-}/13.3%ZrO_2/MCM-41	972.3	0.69	29.4
SO_4^{2-}/26.7%ZrO_2/MCM-41	834.0	0.64	29.2
SO_4^{2-}/41.0%ZrO_2/MCM-41	687.5	0.58	29.1
SO_4^{2-}/48.5%ZrO_2/MCM-41	499.0	0.40	29.1
SO_4^{2-}/ZrO_2	100.5	0.10	—[a]
PMSZM/5.4%ZrO_2	1128.1	0.95	31.3
PMSZM/13.4%ZrO_2	998.7	0.87	31.2
PMSZM/26.7%ZrO_2	920.5	0.78	31.2
PMSZM/41.0%ZrO_2	765.2	0.63	31.1
PMSZM/48.5%ZrO_2	684.2	0.53	31.0

[a] Not detectable.

traditional SO_4^{2-}/ZrO_2 solid acid. The BET surface area and pore volume of MCM-41 and all SO_4^{2-}/ZrO_2/MCM-41 samples show a descending tendency: MCM-41 > SO_4^{2-}/5.5%ZrO_2/MCM-41 > SO_4^{2-}/13.3%ZrO_2/MCM-41 > SO_4^{2-}/26.7%ZrO_2/MCM-41 > SO_4^{2-}/41.0%ZrO_2/MCM-41 > SO_4^{2-}/48.5%ZrO_2/MCM-41 $\gg$ SO_4^{2-}/ZrO_2. SO_4^{2-}/ZrO_2 material has a very small BET surface area of about 100.5 m^2/g and an extremely low pore volume of 0.10 cm^3/g. SO_4^{2-}/ZrO_2/MCM-41 samples with ZrO_2 loadings of $\leq$41.0 wt% possess a large BET surface area of $\geq$687.5 m^2/g and a high pore volume of $\geq$0.58 cm^3/g. When ZrO_2 loading is increased to 48.5 wt%, the BET surface area and pore volume of the resulting SO_4^{2-}/48.5%ZrO_2/MCM-41 reduce to 499 m^2/g and 0.40 cm^3/g, respectively. However, all SO_4^{2-}/ZrO_2/MCM-41 samples display a fairly uniform mesopore size distribution centered at about 29.1–29.5 Å. This demonstrates the advantages of using uniform mesoporous material having a high BET surface area as a support for solid acid catalysts. The pore diameter of the SO_4^{2-}/ZrO_2/MCM-41 samples is ca. 2 Å less than that of the siliceous MCM-41 support, indicating that the supported ZrO_2 has been dispersed onto mesopores of MCM-41. The reduction in the BET surface area and pore volume of the samples with an increase in ZrO_2 loading from 5.5 to 48.5% is much more remarkable than that of their pore sizes, indicating a partial blockage of mesopores in the MCM-41 support by excessive ZrO_2.

The BET surface area and pore volume of physically mixed PMSZM/ZrO_2 samples also display a similar reduction to the increase of the ZrO_2 amount but are somewhat higher than those of the SO_4^{2-}/ZrO_2/MCM-41 sample with an identical ZrO_2 amount. Along with increased ZrO_2 amounts from 0 to 48.5 wt%, the BET surface area and pore volume of the resulting mixtures drastically decrease from 1311.0 to 684.2 m^2/g and from 1.03 to 0.53 cm^3/g, respectively. Their pore sizes do not show any notable reduction as compared to that of Si-MCM-41; however, a small drop in pore size to 31.0 Å was shown by increasing the ZrO_2 amount from 0 to 48.5 wt%. This is reasonable because PMSZM/ZrO_2 samples are prepared through mechanically grinding a mixture of SO_4^{2-}/ZrO_2 and MCM-41. The increase of the ZrO_2 amount does not affect the pore diameter of MCM-41 severely, but it reduces the BET surface area and pore volume of the resulting materials. The results indicate that for PMSZM/ZrO_2 samples, the thermal treatment at high temperature induces the interaction between ZrO_2 and SiO_2 as well as the thermal shifting of ZrO_2 into mesopores; however, this effect on the mesostructure is still weaker than that in the case of the SO_4^{2-}/ZrO_2/MCM-41 samples.

The change in the shape of isotherms for all SO_4^{2-}/ZrO_2/MCM-41 samples is depicted in Fig. 5. A sharp inflection can be observed on the isotherms of siliceous MCM-41 and SO_4^{2-}/ZrO_2/MCM-41 samples at relative pressures between $p/po = 0.25$ and 0.40, showing that these materials have typical mesoporous structures. The appearance of a small *Type H1* hysteresis loop on the isotherm of MCM-41 can be associated with porous material which consists of agglomerates or compacts of approximately uniform spheres in a fairly regular array and hence having a narrow distribution of pore size (47). For SO_4^{2-}/ZrO_2/MCM-41 samples, the

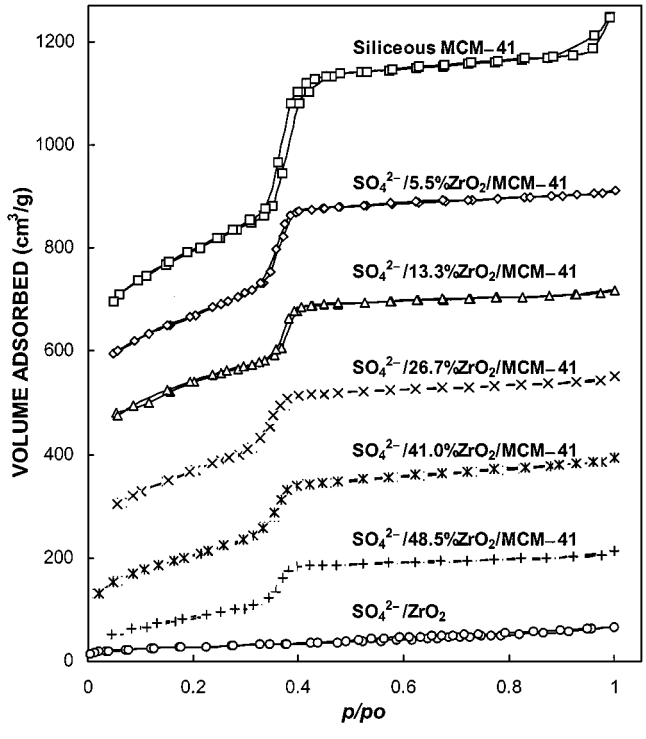

FIG. 5. The effect of ZrO_2 loading on the nitrogen adsorption–desorption isotherms of SO_4^{2-}/ZrO_2/MCM-41 samples.

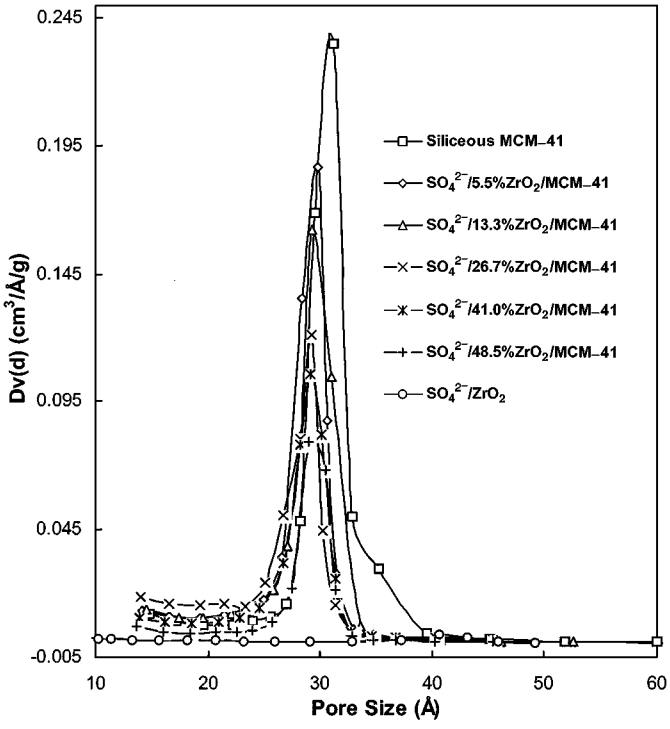

FIG. 6. The effect of ZrO_2 loading on the pore size of SO_4^{2-}/ZrO_2/MCM-41 samples.

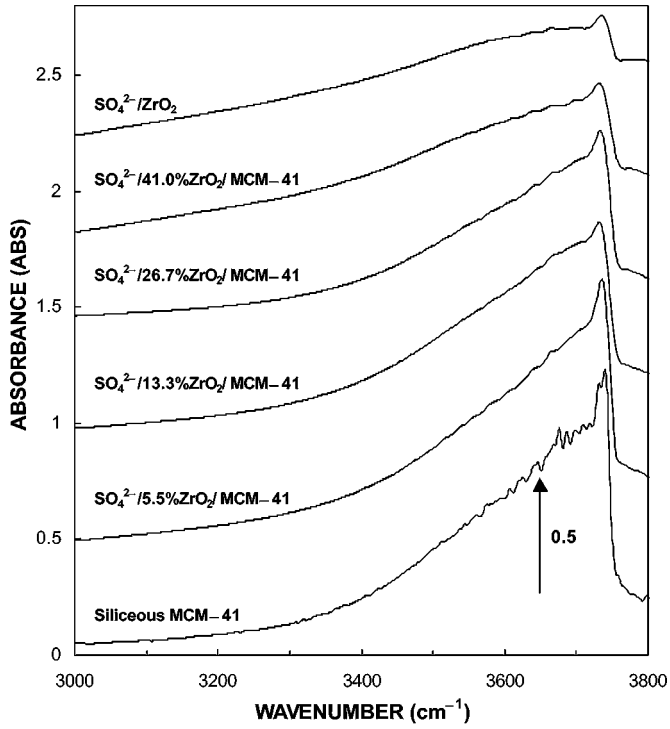

FIG. 7. The effect of ZrO_2 loading on the coverage of surface hydroxyl groups of SO_4^{2-}/ZrO_2/MCM-41 samples.

absence of a hysteresis loop on the isotherms reveals the uniformity of their mesoporous structures ascribed to the homogeneous dispersion of ZrO_2 on MCM-41. With an increase in ZrO_2 loading, the length of inflection shortens gradually, corresponding to a reduction in the pore volume. Figure 6 shows a marked compression in the pore size distribution as a result of ZrO_2 loading on MCM-41 as listed in Table 1; however, a further decrease cannot be observed even if ZrO_2 loading increases from 5.5 to 48.5%. In the SO_4^{2-}/ZrO_2 sample, no observable inflection on its isotherm and detectable pore size distribution shows its nonporous characteristics.

3.2. The Surface Hydroxyl Coverage on SO_4^{2-}/ZrO_2 and SO_4^{2-}/ZrO_2/MCM-41 Materials

Figure 7 shows the FTIR spectra between 3800 and 3000 cm^{-1} of the calcined Si-MCM-41, SO_4^{2-}/ZrO_2, and SO_4^{2-}/ZrO_2/MCM-41 materials evacuated (10^{-6} mbar) at 300°C. The hydroxyl region of the FTIR spectrum of mesoporous siliceous MCM-41 has been investigated previously (48), where the bands around 3742, 3732, 3720–3690, 3680–3620, and 3600–3450 cm^{-1} were assigned, respectively, to isolated silanols and to associated hydroxyls with different degrees of hydrogen bonding. The absorbance in these regions for siliceous MCM-41 is clearly evident in the present work, in which many bands at about 3742, 3732, 3720, 3710, 3700, 3687, 3675, 3647, 3621, 3608, 3575, and 3521 cm^{-1}, etc. are observed. On the deposition of ZrO_2, there is a clear decrease, around 3742 cm^{-1}, in the absorbance assigned to isolated silanols, and in the region around 3680–3620 cm^{-1}, previously assigned to hydrogen bonding in small clusters of silanols. The decreased absorbance in the aforementioned spectral regions is, presumably, due to the dispersion of ZrO_2 on mesopores and the chemical interaction of $Zr(OPr^n)_4$ with silanols as depicted in Scheme 1. Interaction with these hydroxyls has been reported in the case of silylation reactions (49). In the synthesis of SO_4^{2-}/ZrO_2/MCM-41 samples Scheme 1 shows the possible chemical interaction, decreasing surface–OH coverage, pore volume, and pore diameter.

The absorbance in the 3732-cm^{-1} region associated with very weakly hydrogen-bonded silanols is always observable in all SO_4^{2-}/ZrO_2/MCM-41 samples; however, its intensity appears to be gradually reduced with increased ZrO_2 loading. This suggests that these hydroxyls which are associated with defects in the walls of siliceous MCM-41 materials are not easily available to larger $Zr(OPr^n)_4$ molecules.

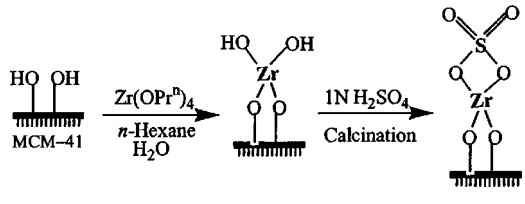

SCHEME 1

TABLE 2

Comparison of Coverage of Surface Hydroxyl Groups and Sulfate Content of Siliceous MCM-41, SO_4^{2-}/ZrO_2, and SO_4^{2-}/ZrO_2/MCM-41 Samples[a]

Sample	–OH coverage (area fraction %)	Weight loss (wt%)	Sulfate content (wt%)
Siliceous MCM-41	100	0	0
SO_4^{2-}/5.5%ZrO_2/MCM-41	72.0	1.46	1.75
SO_4^{2-}/13.3%ZrO_2/MCM-41	61.5	2.57	3.08
SO_4^{2-}/26.7%ZrO_2/MCM-41	51.0	4.86	5.83
SO_4^{2-}/41.0%ZrO_2/MCM-41	40.4	7.58	9.10
SO_4^{2-}/ZrO_2	25.1	5.81	6.97

[a] All samples were calcined at 600°C for 3 h before measurements.

Obviously, after the deposition of ZrO_2 on MCM-41, there appear to be gradually reduced intensities (peak area) for all hydroxyl vibrations. Table 2 shows a reduction of the relative coverage of surface hydroxyl groups from 100% of MCM-41 to 25.1% of SO_4^{2-}/ZrO_2. For siliceous MCM-41 and SO_4^{2-}/5.5–41.0%ZrO_2/MCM-41 samples, the relationship between –OH coverage and SiO_2 mol% calculated theoretically in terms of composition is notably different from that determined experimentally as shown in Fig. 8. When the SiO_2 content is decreased to 66 mol% in the samples, the calculated –OH coverage merely, reduces linearly to 76.9%; however, the determined –OH coverage drastically drops to 40.4% in a concave manner. The big drop in –OH coverage mainly concentrates on SO_4^{2-}/ZrO_2/MCM-41 with $\leq$13.3 wt% ZrO_2, i.e., with a $\geq$90.9 mol% SiO_2 content. In this case, the –OH coverage on the surface of sample has reduced to 61.5% of Si-MCM-41. This confirms that the reduction of the surface –OH coverage on SO_4^{2-}/ZrO_2/MCM-41 materials is probably due to the high dispersion of ZrO_2 and the chemical interaction between ZrO_2 and Si–OH as depicted in Scheme 1. A continuous increase of ZrO_2 loading further enhances the aforementioned effects. The increase of ZrO_2 loading on MCM-41 results in the reduction of surface hydroxyls to a great extent, further enhancing the hydrophobicity of the SO_4^{2-}/ZrO_2/MCM-41 materials. Thus, the order of hydrophobicity of the samples can be arranged into SO_4^{2-}/ZrO_2 > SO_4^{2-}/41.0%ZrO_2/MCM-41 > SO_4^{2-}/26.7%ZrO_2/MCM-41 > SO_4^{2-}/13.3% ZrO_2/MCM-41 > SO_4^{2-}/5.5%ZrO_2/MCM-41 > Si-MCM-41. It is well known that the hydrophobicity is rather important for the high activity of the SO_4^{2-}/ZrO_2 acid catalyst in the synthesis of MTBE, as the adsorption of water will lead to the decrease of acidity of such solid acid catalysts (3, 44).

3.3. The Sulfate Amount in SO_4^{2-}/ZrO_2/MCM-41 Catalysts

The *in situ* FTIR spectrum of SO_4^{2-}/ZrO_2 in Fig. 9 measured after evacuation at 400°C for 5 h, shows an absorption band at ca. 1378 cm^{-1}, corresponding to the asymmetric

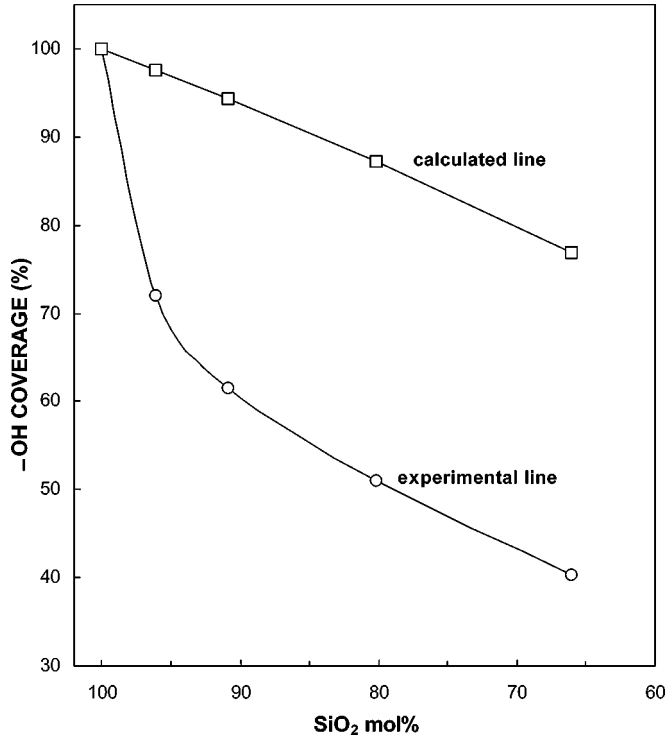

FIG. 8. The comparison of the calculated –OH coverage to the determined –OH coverage with SiO_2 mol%.

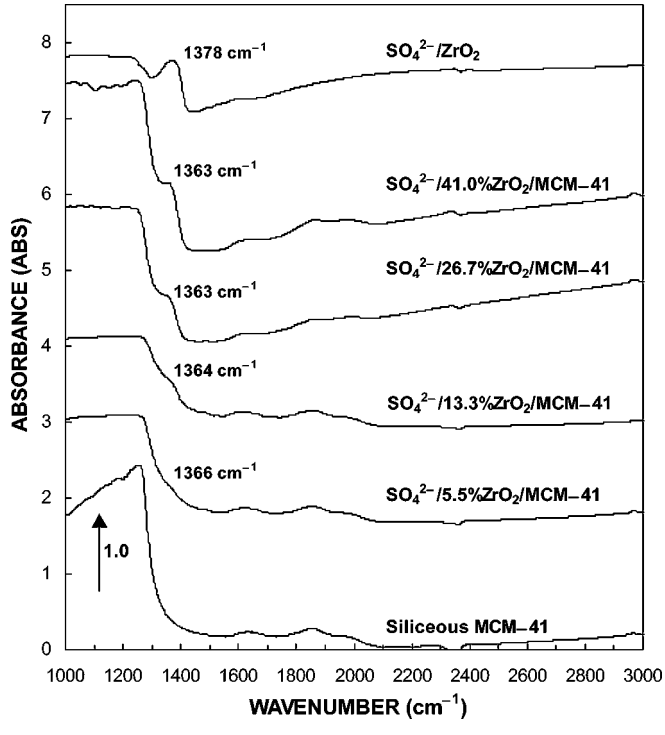

FIG. 9. The effect of ZrO_2 loading on the S=O vibrational bands of SO_4^{2-}/ZrO_2/MCM-41 samples.

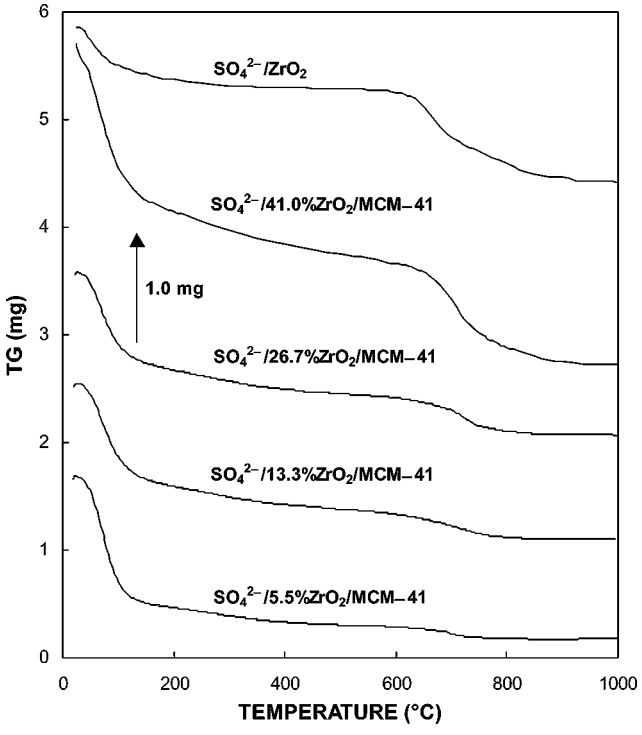

FIG. 10. The effect of ZrO_2 loading on the weight loss of SO_4^{2-}/ZrO_2/MCM-41 samples.

stretching frequency of the covalent S=O band; this band is often regarded as the characteristic band of SO_4^{2-} on promoted solid acids (2, 4, 6, 12). Such a covalent S=O band cannot be observed at all in the Si-MCM-41 support, while only a shoulder band is observed at ca. 1366 cm^{-1} for a low 5.5% ZrO_2 loading on Si-MCM-41. With increased ZrO_2 loading, 5.5 to 41.0% this band becomes more intense and shifts to ca. 1363 cm^{-1}. The shifting in the SO_4^{2-}/ZrO_2/MCM-41 materials is attributed to the influence of the interaction between ZrO_2 and framework SiO_2. Very clearly, the enhancement of this band is proportional to ZrO_2 loading on Si-MCM-41. This is because the high ZrO_2 loading can interact with more sulfate anions to form the high density of covalent S=O absorbance, an explanation that has been proven by IR spectra (Fig. 9) and sulfate content (Table 2).

TGA profiles in Fig. 10 show that SO_4^{2-}/ZrO_2 and SO_4^{2-}/ZrO_2/MCM-41 materials display common double-stage weight-loss features: the first below 200°C (due to the evaporation of physically adsorbed water and other molecules) and the second between 580 and 900°C (attributed to the removal of SO_4^{2-} species interacting with ZrO_2), regardless of the ZrO_2 loading. The similarities of the decomposition temperature for these samples indicate that the distribution of SO_4^{2-} species on SO_4^{2-}/ZrO_2 and SO_4^{2-}/ZrO_2/MCM-41 is quite similar. For the SO_4^{2-}/ZrO_2/MCM-41 samples, with a decrease in ZrO_2 loading from 41.0 to 5.5%, the weight-loss step between 600 and 750°C shortens gradually, corresponding to the decrease of sulfate content in the samples as shown in Table 2. It should be mentioned that after calcination at 600°C for Si-MCM-41 immersed with 1 N H_2SO_4 solution, no weight loss could be detected from its TG curve between 600 and 1000°C. This further confirms that the sulfate ions in SO_4^{2-}/ZrO_2/MCM-41 samples come from the interaction of ZrO_2 and sulfate ions.

Based on the amount of weight loss, the sulfate content contained in SO_4^{2-}/ZrO_2 and SO_4^{2-}/ZrO_2/MCM-41 samples has been calculated in Table 2. The calculation of the sulfate content in weight percentage from the weight loss in the TGA experiment requires the knowledge of the decomposition mechanism of sulfate. White *et al.* (50) reported that in the SO_4^{2-}/ZrO_2 sample, SO_2 and O_2 are formed at a the ratio of 2 : 1 in the TGA experiment, suggesting the formal loss of SO_3; i.e., the SO_4^{2-} content would be 1.2 times the weight loss. SO_4^{2-}/ZrO_2 and SO_4^{2-}/41.0%ZrO_2/MCM-41 calcined at 600°C contain 6.97 and 9.10 wt% sulfate ions, respectively. When ZrO_2 loading is reduced, the content of sulfate ions contained in the resulting SO_4^{2-}/ZrO_2/MCM-41 samples shows a gradual reduction. However, even if the ZrO_2 content is reduced to 5.5%, the resulting SO_4^{2-}/5.5%ZrO_2/MCM-41 still adsorbs 1.75 wt% of sulfate anions equivalent to one-quarter of the sulfate content in SO_4^{2-}/ZrO_2. The capability of adsorbing sulfate anions for all sulfated ZrO_2 samples in Table 2 can be placed in the following ascending order: SO_4^{2-}/5.5%ZrO_2/MCM-41 < SO_4^{2-}/13.3%ZrO_2/MCM-41 < SO_4^{2-}/26.7%ZrO_2/MCM-41 < SO_4^{2-}/ZrO_2 < SO_4^{2-}/41.0%ZrO_2/MCM-41. ICP analyses have shown that these SO_4^{2-}/ZrO_2/ MCM-41 samples contain ZrO_2 amounts to be nearly 2/5, 4/15, 2/15, or 1/18 that in SO_4^{2-}/ZrO_2, respectively. As a result, we conclude that the highly dispersed ZrO_2 on MCM-41 can expose more ZrO_2 and adsorb more SO_4^{2-} anions than bulk crystalline ZrO_2. The sulfate content in SO_4^{2-}/ZrO_2/MCM-41 samples is proportional to the ZrO_2 loading, showing that the change of intensity of the covalent S=O band with ZrO_2 loading is simply decided by the sulfate content in the samples. The respective sulfate content in PMSZM/ZrO_2 samples is 0.40, 1.00, 2.00, and 3.07 wt%, corresponding to the ZrO_2 amounts of 5.4, 13.4, 26.7, and 41.0 wt%, much lower than those in the SO_4^{2-}/ZrO_2/MCM-41 samples. This is because the sulfate content in the PMSZM/ZrO_2 samples can be merely related to the sulfate content of SO_4^{2-}/ZrO_2 as one of two components in the physical mixture of SO_4^{2-}/ZrO_2 and MCM-41.

3.4. The Distribution of S, Zr, and Si Atoms in SO_4^{2-}/ZrO_2, SO_4^{2-}/ZrO_2/MCM-41 and PMSZM/ZrO_2 Samples

The SEM–EDX technique was used to measure the distribution of S, Zr, Si, and O atoms in the SO_4^{2-}/ZrO_2, SO_4^{2-}/ZrO_2/MCM-41, and PMSZM/ZrO_2 samples. Their

TABLE 3

Comparison of S : Zr : Si Atomic Ratio of SO_4^{2-}/ZrO_2/MCM-41 and PMSZM/ZrO_2 Samples

Sample	S : Zr : Si[a] (atomic ratio)	S : Zr : Si[b] (atomic ratio)
SO_4^{2-}/5.5%ZrO_2/MCM-41	1:2.45:84.85	1:7.08:54.06
SO_4^{2-}/13.3%ZrO_2/MCM-41	1:3.36:43.42	1:7.46:25.86
SO_4^{2-}/26.7%ZrO_2/MCM-41	1:3.51:34.72	1:8.84:21.30
SO_4^{2-}/41.0%ZrO_2/MCM-41	1:3.57:8.77	1:9.78:12.02
SO_4^{2-}/ZrO_2	1:10.40:0	1:16.84:0
PMSZM/5.4%ZrO_2	1:10.46:374.92	(S% = 0)
PMSZM/13.4%ZrO_2	1:10.45:137.10	(S% = 0)
PMSZM/26.7%ZrO_2	1:10.39:57.01	1:18.67:43.29
PMSZM/41.0%ZrO_2	1:10.40:29.13	1:17.17:19.29

[a] Calculated based on TG and ICP analyses.
[b] Determined atomic percentage by SEM–EDX analysis.

S : Zr : Si atomic ratios are listed in Table 3, where the data in the first column are calculated based on TG and ICP analyses; those in the second column are determined by SEM–EDX analysis. Note that EDX analysis did not detect the presence of other elements such as F, Cl, Na, Al, etc., in all sulfated ZrO_2 samples, possibly due to the fact that the content in these samples is lower than the determination limitation of EDX analysis. Since the highly exposed ZrO_2 in SO_4^{2-}/ZrO_2/MCM-41 samples adsorb more SO_4^{2-} anions than bulk crystalline ZrO_2 in SO_4^{2-}/ZrO_2, the calculated atomic ratios of S : Zr : Si (in the first column) in these samples are higher than those in SO_4^{2-}/ZrO_2 and PMSZM/ZrO_2 samples. For SO_4^{2-}/ZrO_2/MCM-41 samples, the calculated S : Zr ratios decrease from 1 : 2.45 to 1 : 3.57 with increased ZrO_2 loading from 5.5 to 41.0 wt%, while for SO_4^{2-}/ZrO_2 and PMSZM/ZrO_2 samples, this value is almost fixed at about 1 : 10.40 regardless of the ZrO_2 amount. This is acceptable because PMSZM/ZrO_2 samples are prepared through physically grinding the mixture of SO_4^{2-}/ZrO_2 and MCM-41 in different ZrO_2 ratios.

However, for all samples in Table 3, the S : Zr ratios determined by EDX analysis (in the second column) are lower than those calculated in the first column. For SO_4^{2-}/ZrO_2, the calculated value is 1 : 10.40, while the determined value decreases to 1 : 16.84. For PMSZM/26.7%ZrO_2 and PMSZM/41.0%ZrO_2, the calculated value equals that of SO_4^{2-}/ZrO_2, while the determined value becomes 1 : 18.67 and 1 : 17.17, still similar to that of SO_4^{2-}/ZrO_2. However, for PMSZM/5.4%ZrO_2 and PMSZM/13.4%ZrO_2, the presence of sulfur cannot be determined at all by EDX, possibly because the sulfur content in both samples is lower than the determination limitation of EDX analysis. In contrast, the S : Zr : Si ratios in all SO_4^{2-}/ZrO_2/MCM-41 samples can be well determined by EDX. Particularly, for SO_4^{2-}/5.5%ZrO_2/MCM-41 and SO_4^{2-}/13.3%ZrO_2/MCM-41, the S : Zr : Si ratios are determined by EDX to be 1 : 7.08 : 54.06, and 1 : 7.46 : 25.86. This evidence confirms that the sulfur content in the SO_4^{2-}/ZrO_2/MCM-41 sample is higher than that in the PMSZM/ZrO_2 sample with the same ZrO_2 amount. It should be pointed out that Sulfur Ka1 and Zirconium La1 distribution spectra determined by SEM–EDX analysis have clearly shown homogeneous distribution of S and Zr atoms in these samples; therefore the fact that lower S : Zr ratios were determined rather than calculated further indicates that the sulfur distribution in these samples be less on the surface than in the bulk phase.

3.5. The Surface Acidity of All Sulfated ZrO_2 Catalysts

The presence of Brønsted and Lewis acid sites on the surface of SO_4^{2-}/ZrO_2, SO_4^{2-}/ZrO_2/MCM-41 and PMSZM/ZrO_2 samples has been measured *in situ* by pyridine adsorption IR spectra. FTIR spectra in Fig. 11 show that SO_4^{2-}/ZrO_2 and SO_4^{2-}/ZrO_2/MCM-41 catalysts contain strong Brønsted acidity (at 1540 cm^{-1}) and Lewis acidity (at 1445 cm^{-1}). The surface of Si-MCM-41 does not contain any Brønsted and Lewis acidities. In the spectrum of Si-MCM-41, the absorbance at about 1440 cm^{-1} associated with the absorbance at about 1600 cm^{-1} can be ascribed to hydrogen-bonded pyridine, rather than Lewis acidity usually monitored by the bimodal absorbances at about 1445 and 1580 cm^{-1}. Once Si-MCM-41 is loaded with ZrO_2, strong Brønsted and Lewis acidities emerge

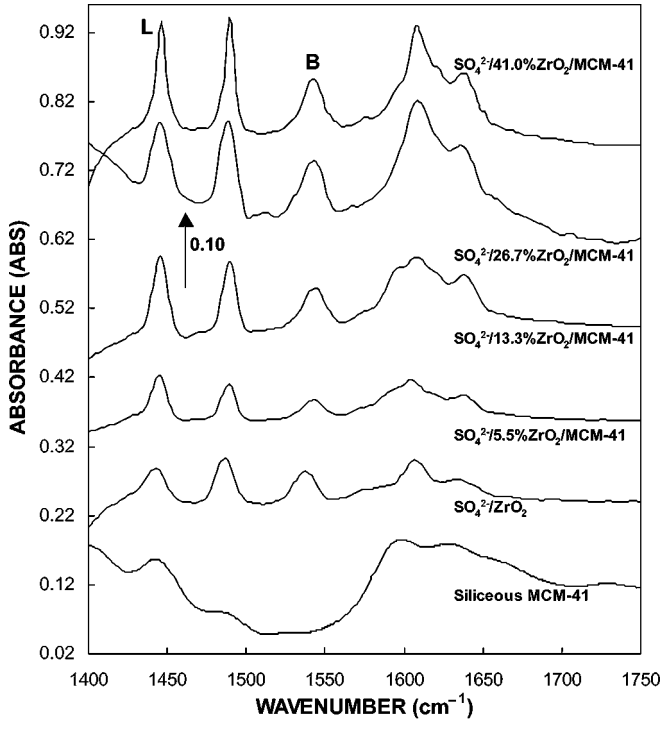

FIG. 11. The effect of ZrO_2 loading on the pyridine adsorption FTIR spectra of SO_4^{2-}/ZrO_2/MCM-41 samples.

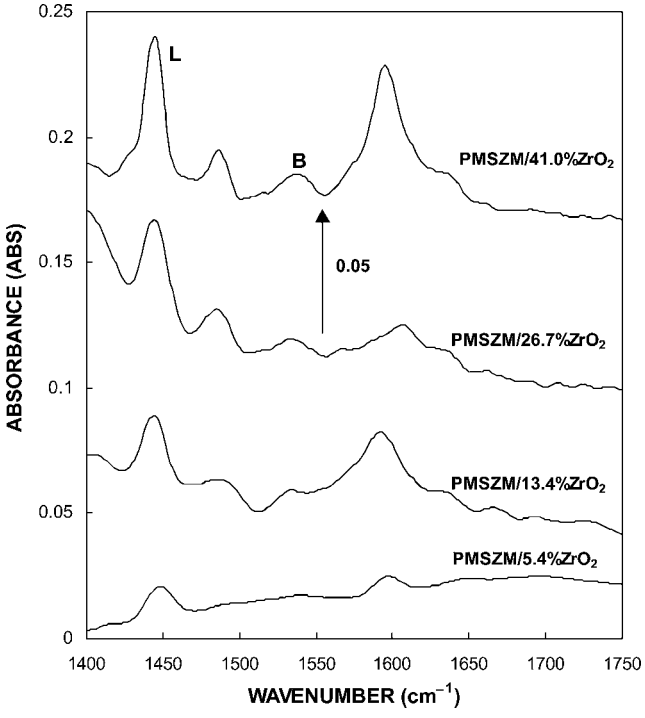

FIG. 12. The effect of ZrO_2 amount on the pyridine adsorption FTIR spectra of PMSZM/ZrO_2 samples.

on the SO_4^{2-}/ZrO_2/MCM-41 catalysts, and both gradually strengthen with increased ZrO_2 loading from 5.5 to 41.0 wt%, while four PMSZM/ZrO_2 samples contain very weak Brønsted and Lewis acidities as shown in Fig. 12. On the surface of PMSZM/5.4%ZrO_2, the Brønsted acid site is unobservable; only one weak absorbance appears at about 1445 cm^{-1} assigned to the Lewis acid site. Along with increased ZrO_2 amounts in PMSZM/ZrO_2 samples, the number of Brønsted acid sites shows a rather slow increase. There is one possible reason for these observations. For SO_4^{2-}/ZrO_2/MCM-41 catalysts, ZrO_2 has been uniformly dispersed onto mesopores of MCM-41 through chemical liquid deposition, therefore their surfaces expose more ZrO_2 to interact with H_2SO_4 molecules forming more Brønsted and Lewis acid sites. For PMSZM/ZrO_2 catalysts, only SO_4^{2-}/ZrO_2 acid sites with a limited number are diluted into inert MCM-41 solids through physical mixing, and no more additional acid sites are formed.

Brønsted and Lewis acidities in Figs. 11 and 12 have been quantified into the integrated areas of the peaks at 1540 and at 1445 cm^{-1}, respectively, as listed in Table 4. All SO_4^{2-}/ZrO_2/MCM-41 catalysts except SO_4^{2-}/5.5% ZrO_2/MCM-41 contain more Brønsted and Lewis acid sites than traditional SO_4^{2-}/ZrO_2. The Brønsted and Lewis acids and the B/L value of SO_4^{2-}/ZrO_2 and SO_4^{2-}/ZrO_2/MCM-41 samples can be placed in the following order: Si-MCM-41 < SO_4^{2-}/5.5%ZrO_2/MCM-41 < SO_4^{2-}/ZrO_2 < SO_4^{2-}/13.3% ZrO_2/MCM-41 < SO_4^{2-}/26.7%ZrO_2/MCM-41 ≈ SO_4^{2-}/ 41.0%ZrO_2/MCM-41. This sequence is strikingly different from the capability of adsorbing sulfate ions of these materials, reflecting that there are many complicated factors that influence the surface acidities of the catalysts, such as ZrO_2 loading, the crystalline phase of ZrO_2, the capability of adsorbing sulfate ions, and the dispersion of ZrO_2 on the support. For SO_4^{2-}/ZrO_2/MCM-41 materials, even though the ZrO_2 loading is as low as 5.5 wt%, Brønsted and Lewis acid sites can still form, where Brønsted acidity is 0.41 and Lewis acidity is 0.81. The acidity of the SO_4^{2-}/ZrO_2/MCM-41 samples first displays a clear increase with increased ZrO_2 loading from 5.5 to 26.7 wt% and then gradually approaches an equilibrium value with a further increase of ZrO_2 loading to 41.0 wt%. The Brønsted and Lewis acidities and the B/L value on SO_4^{2-}/26.7%ZrO_2/MCM-41 and SO_4^{2-}/41.0%ZrO_2/MCM-41 reach about 1.20, 1.40, and

TABLE 4

Pyridine Adsorption Data on Si-MCM-41, SO_4^{2-}/ZrO_2, SO_4^{2-}/ZrO_2/MCM-41, and PMSZM/ZrO_2 Samples

Sample	B acid[a] (at 1540 cm^{-1})	L acid[a] (at 1445 cm^{-1})	B/L	ZrO_2[b] crystal phase
Siliceous MCM-41	0	0	0	
SO_4^{2-}/5.5%ZrO_2/MCM-41	0.41	0.81	0.51	amorphous
SO_4^{2-}/13.3%ZrO_2/MCM-41	0.90	1.21	0.74	amorphous
SO_4^{2-}/26.7%ZrO_2/MCM-41	1.20	1.40	0.86	tetragonal
SO_4^{2-}/41.0%ZrO_2/MCM-41	1.21	1.43	0.85	tetragonal
SO_4^{2-}/ZrO_2	0.70	1.00	0.70	tetragonal
PMSZM/5.4%ZrO_2	0.016	0.24	0.07	tetragonal
PMSZM/13.4%ZrO_2	0.026	0.43	0.06	tetragonal
PMSZM/26.7%ZrO_2	0.062	0.60	0.10	tetragonal
PMSZM/41.0%ZrO_2	0.16	0.88	0.18	tetragonal

[a] Brønsted and Lewis acidities are quantified into integrated areas of the absorbances at 1540 and at 1445 cm^{-1}, respectively.

[b] The crystalline phase of ZrO_2 is detected by XRD.

TABLE 5

Catalytic Activities of SO_4^{2-}/ZrO_2, SO_4^{2-}/ZrO_2/MCM-41, and PMSZM/ZrO_2 Catalysts[a]

Catalyst	Conversion (mol%)	Selectivity (%)	Optimal temperature (°C)
SO_4^{2-}/ZrO_2	98.0	100	140
SO_4^{2-}/41.0%ZrO_2/MCM-41	98.6	100	140
SO_4^{2-}/26.7%ZrO_2/MCM-41	98.1	100	140
SO_4^{2-}/13.3%ZrO_2/MCM-41	97.9	100	150
SO_4^{2-}/5.5%ZrO_2/MCM-41	95.6	100	160
PMSZM/41.0%ZrO_2	90.5	100	180
PMSZM/26.7%ZrO_2	81.5	100	190
PMSZM/13.4%ZrO_2	75.0	100	220
PMSZM/5.4%ZrO_2	70.6	100	240

[a] The gas–solid phase synthesis of MTBE from MeOH and Bu^{t}OH was carried out in a continuous fixed-bed reactor: 0.20 g of the catalyst, a helium flow of 13 ml/min, a mixture reactant of MeOH and Bu^{t}OH with a molar ratio of 10:1, and a WHSV kept at 10 h^{-1}.

0.85. This demonstrates that there is an optimum of ZrO_2 loading on MCM-41 to achieve an ideal mesoporous acid catalyst, rather than using an infinite amount of ZrO_2 loading. Since the sulfate content in SO_4^{2-}/ZrO_2/MCM-41 samples is proportional to the ZrO_2 loading, their acidity is a direct function of the sulfate content and the ZrO_2 loading, in agreement with the observation reported by Quiroga *et al.* (44).

In contrast to SO_4^{2-}/ZrO_2 and SO_4^{2-}/ZrO_2/MCM-41 samples, all PMSZM/ZrO_2 samples contain extremely weak Brønsted and Lewis acidities on their surfaces. Brønsted and Lewis acidities on PMSZM/ZrO_2 samples also display a gradual increase with increasing ZrO_2 amounts; however, when the ZrO_2 amount is increased to 41.0 wt%, its Brønsted and Lewis acidities increase to only 0.16 and 0.88, respectively. In this case, the Lewis acidity of PMSZM/41.0%ZrO_2 is comparable to that of SO_4^{2-}/5.5%ZrO_2/MCM-41, but its Brønsted acidity is merely equivalent to two-fifths of the latter. This comparison suggests that SO_4^{2-}/ZrO_2/MCM-41 material synthesized through a chemical process contains more acid sites than PMSZM/ZrO_2 prepared through physically grinding the mixture of conventional SO_4^{2-}/ZrO_2 and MCM-41. This further suggests that physical mixing is not advantageous over increasing the surface acidities of sulfated ZrO_2-supported mesoporous acidic materials, largely retarding the catalytic activity of the resulting catalysts.

A correlation between the acidity and the crystalline phase of ZrO_2 detected by XRD cannot be obtained for all sulfated ZrO_2 catalysts. Figures 3 and 4 and Table 4 demonstrate that ZrO_2 presents as an amorphous solid in SO_4^{2-}/5.5%ZrO_2/MCM-41 and SO_4^{2-}/13.3%ZrO_2/MCM-41, while it appears as a tetragonal crystalline phase in SO_4^{2-}/26.7%ZrO_2/MCM-41, SO_4^{2-}/41.0%ZrO_2/MCM-41, SO_4^{2-}/ZrO_2, and all PMSZM/ZrO_2 samples. However, the number of surface acid sites of SO_4^{2-}/5.5%ZrO_2/MCM-41 and SO_4^{2-}/13.3%ZrO_2/MCM-41 is much greater than that of all PMSZM/ZrO_2 samples. It seems that the formation of tetragonal crystalline ZrO_2 can be partially ascribed to the dense stacking of ZrO_2 clusters or aggregates due to quite poor dispersion in high ZrO_2 loading.

3.6. The Catalytic Activity of All Sulfated ZrO_2 Catalysts

For the gas–solid phase synthesis of MTBE from MeOH and Bu^{t}OH in a continuous fixed-bed reactor, a 13-ml/min helium flow has to be introduced into the reactor together with the reactants in order to maintain a stable operation and to speed up the adsorption–desorption processes. The dependence of activity of all sulfated ZrO_2 catalysts on the reaction temperature is depicted in Fig. 13. Clearly, this reaction is very sensitive to the change in reaction temperature, where a small temperature gap of only 10°C seriously affects the conversion of Bu^{t}OH. Because of the lack of surface acidities, Si-MCM-41 shows extremely low activity. At temperatures below 160°C, the conversion of Bu^{t}OH to MTBE on Si-MCM-41 is close to 0; even if the temperature is elevated to 250°C, only 25 mol% of Bu^{t}OH can be converted to MTBE. However, SO_4^{2-}/ZrO_2 and all SO_4^{2-}/ZrO_2/MCM-41 catalysts show rather high activities

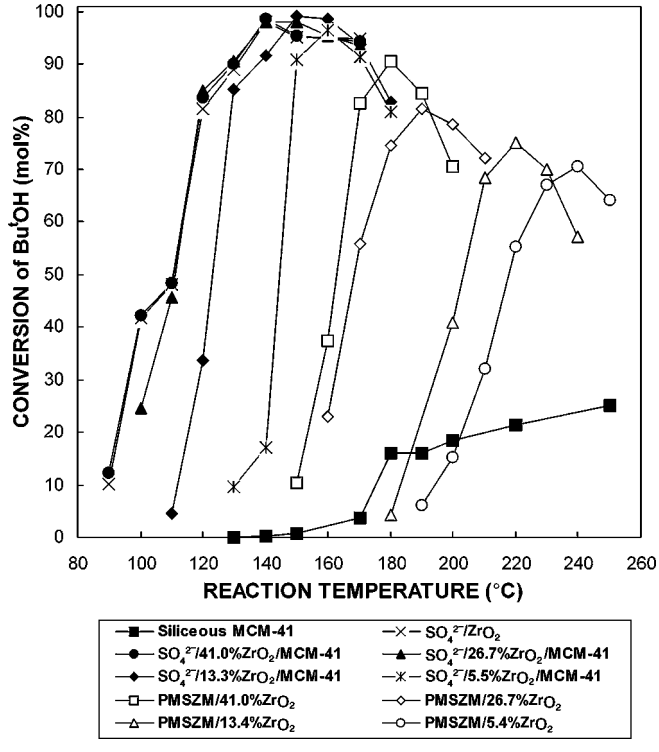

FIG. 13. The effect of the ZrO_2 loading on the activity of SO_4^{2-}/ZrO_2, SO_4^{2-}/ZrO_2/MCM-41, and PMSZM/ZrO_2 catalysts for the gas-phase synthesis of MTBE from MeOH and Bu^{t}OH.

with a selective conversion of >95 mol% Bu^tOH to MTBE at rather low temperatures below 160°C. This result shows that this reaction is a typical acid-catalyzed reaction and these solid acid catalysts are very effective for this reaction. The activity order of all SO_4^{2-}/ZrO_2/MCM-41 catalysts is as follows: $SO_4^{2-}/ZrO_2 \approx SO_4^{2-}/41.0\%ZrO_2$/MCM-41 $\approx SO_4^{2-}/26.7\%ZrO_2$/MCM-41 $> SO_4^{2-}/13.3\%ZrO_2$/MCM-41 $> SO_4^{2-}/5.5\%ZrO_2$/MCM-41 $\gg$ Si-MCM-41. For SO_4^{2-}/ZrO_2/MCM-41 catalysts, the catalytic activity reduces gradually with decreased ZrO_2 loading, in agreement with the decreases in the sulfate amount and surface acidity. $SO_4^{2-}/41.0\%ZrO_2$/MCM-41 shows almost the same high activity as $SO_4^{2-}/26.7\%ZrO_2$/MCM-41 as a result of their same surface acidity. The high activity of the SO_4^{2-}/ZrO_2 acid catalyst may be ascribed to its excellent hydrophobicity and integral tetragonal crystalline ZrO_2 phase. The optimal reaction temperature (in Table 5) observed for achieving the highest conversion shifts gradually to higher temperatures with decreased ZrO_2 loading: SO_4^{2-}/ZrO_2(140°C) $\approx SO_4^{2-}/41.0\%ZrO_2$/MCM-41 (140°C) $\approx SO_4^{2-}/26.7\%ZrO_2$/MCM-41 (140°C) $< SO_4^{2-}/13.3\%ZrO_2$/MCM-41 (150°C) $< SO_4^{2-}/5.5\%ZrO_2$/MCM-41 (160°C).

The on-stream steady activity of SO_4^{2-}/ZrO_2 and SO_4^{2-}/ZrO_2/MCM-41 catalysts in the gas-phase synthesis of MTBE is illustrated in Fig. 14. With an increase in time-on-stream to 110 h, the highly selective conversion of Bu^tOH to MTBE can be maintained almost unchanged on these catalysts, showing the excellent on-stream stability of these catalysts for this reaction. Among these catalysts, $SO_4^{2-}/5.5\%ZrO_2$/MCM-41 shows the lowest conversion activity as a result of the least surface acidity; however, a higher than 95 mol% conversion of Bu^tOH to MTBE can still be realized. This result proposes that under the gas–solid phase reaction conditions, the active sites of these acid catalysts are difficult to be decomposed by the adsorption of water molecules to lose the activity. This might be attributed to the relatively small diffusion hindrance of mesoporous catalysts and their high hydrophobicity. All of these results further elucidate the advantages of using a uniform mesoporous material having a high BET surface area as a support for solid acid catalysts for MTBE synthesis and other acid-catalyzed organic reactions in the future.

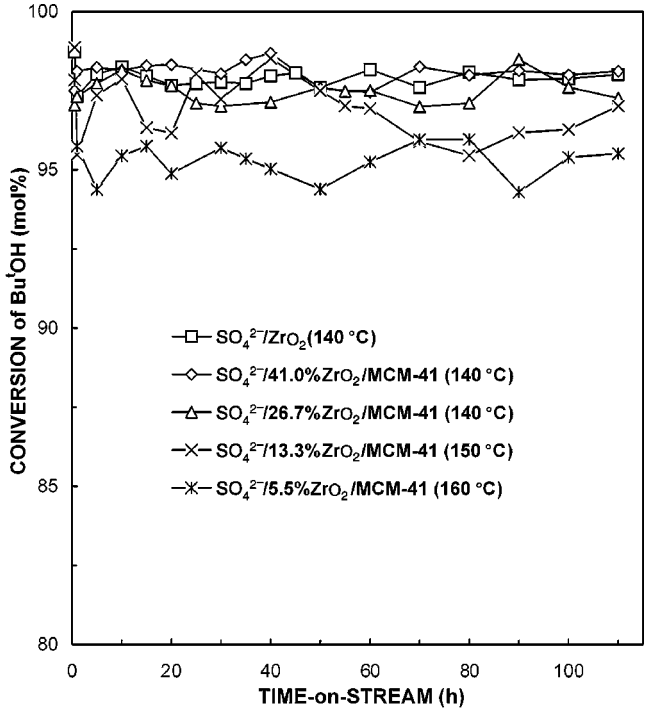

FIG. 14. The stability of on-stream SO_4^{2-}/ZrO_2 and SO_4^{2-}/ZrO_2/MCM-41 catalysts.

However, for the synthesis of MTBE, the activity of PMSZM/ZrO_2 catalysts is lower than that of SO_4^{2-}/ZrO_2/MCM-41 catalysts but much higher than that of siliceous MCM-41, which could be related to the difference of the surface acidity and hydrophobicity of these catalysts. In contrast to SO_4^{2-}/ZrO_2/MCM-41 catalysts, the optimal reaction temperature of PMSZM/ZrO_2 catalysts to achieve the highest conversion of Bu^tOH shifts to much higher temperatures with decreased ZrO_2 loading (in Fig. 13). Their optimal reaction temperatures (in Table 5) are as follows: PMSZM/41.0%ZrO_2 (180°C) < PMSZM/26.7% ZrO_2 (190°C) < PMSZM/13.4%ZrO_2 (220°C) < PMSZM/5.4%ZrO_2 (240°C); however, their highest conversions drop to only 90.5, 81.5, 75.0, and 70.6 mol%. Among PMSZM/ZrO_2 catalysts, PMSZM/41.0% ZrO_2 and PMSZM/26.7%ZrO_2 show a relatively low activity below 160°C, in which the conversion of Bu^tOH reaches only 37.3 and 23.0 mol%. The two other catalysts do not show any activity at temperatures below 160°C. When the ZrO_2 amount is decreased to 5.4 wt%, even though the temperature is elevated to 240°C, merely 70.6 mol% of Bu^tOH is converted to MTBE. Due to the acid-catalyzed nature of MTBE synthesis from methanol and Bu^tOH, in the case of low surface acidity the reaction temperature has to be increased so as to overcome the reaction energy barrier. However, at a high temperature near 200°C side reactions will increase to result in a low conversion of Bu^tOH to MTBE.

4. CONCLUSIONS

The results show that ZrO_2 loading has a striking effect on the intensity of the main XRD reflection [100] peak of Si-MCM-41 support, and this peak weakens proportionally to the increase in ZrO_2 loading. Under high ZrO_2 loading ($\geq$26.7%), a very small amount of ZrO_2 clusters (present as a tetragonal ZrO_2 phase) might be formed inside or

outside the MCM-41 structure. All SO_4^{2-}/ZrO_2/MCM-41 samples display a uniform mesopore size distribution with a high BET surface area >687.5 m^2/g, showing the advantages of using a uniform mesoporous material having a high BET surface area as a support for acid catalysts. The coverage of surface hydroxyl groups on the SO_4^{2-}/ZrO_2/MCM-41 catalysts reduces stepwise with increased ZrO_2 loading, which could be related to the high dispersion of ZrO_2 on MCM-41 and the chemical interaction between ZrO_2 and surface Si–OH groups. The covalent S=O band at 1378 cm^{-1} for SO_4^{2-}/ZrO_2 catalyst shifts to 1363 cm^{-1} for SO_4^{2-}/ZrO_2/MCM-41 catalysts. The shifting is attributed to the influence of the interaction between ZrO_2 and the framework of SiO_2. The sulfate content in SO_4^{2-}/ZrO_2/MCM-41 catalysts is proportional to the ZrO_2 loading. This shows that the change in intensity of the covalent S=O band with ZrO_2 loading is simply decided by the sulfate content in the catalysts. The physically mixed PMSZM/ZrO_2 samples are also found to exert similar effects on the mesostructure, BET surface area, pore size, and surface acidity with varying ZrO_2 amounts. However, Brønsted and Lewis acidities in PMSZM/ZrO_2 are far weaker than those in SO_4^{2-}/ZrO_2/MCM-41 samples.

SO_4^{2-}/ZrO_2 and all SO_4^{2-}/ZrO_2/MCM-41 catalysts show rather high activities with a selective conversion of >95 mol% Bu^tOH to MTBE at rather low temperatures below 160°C. With an increase of time-on-stream to 110 h, the highly selective conversion of Bu^tOH to MTBE can be kept almost unchanged on these sulfated ZrO_2 catalysts, showing the excellent on-stream stability of these catalysts for this reaction. However, the catalytic activity of PMSZM/ZrO_2 catalysts for this reaction is rather low, and the optimal reaction temperature to achieve the highest conversion is much higher than that of the SO_4^{2-}/ZrO_2/MCM-41 catalysts. Particularly, for the PMSZM/5.4%ZrO_2 catalyst, even if the temperature is increased to 240°C, only 70.6 mol% of Bu^tOH is converted to MTBE; however, the SO_4^{2-}/5.5%ZrO_2/MCM-41 catalyst shows a high catalytic activity with >95 mol% conversion at 160°C. This could be related to the difference in the surface acidity and hydrophobicity of these catalysts.

REFERENCES

1. Arata, K., *Adv. Catal.* **37**, 165 (1990).
2. Song, X. M., and Sayari, A., *Catal. Rev.—Sci. Eng.* **38**, 329 (1996).
3. Yadav, G. D., and Nair, J. J., *Micropor. & Mesopor. Mater.* **33**, 1 (1999).
4. Riemer, T., Spielbauer, D., Hunger, M., Mekhemer, G. A. H., and Knozinger, H., *Chem. Commun.* 1181 (1994).
5. Corma, A., Fornes, V., Juanrajadell, M. I., and Nieto, J. M. L., *Appl. Catal.* **116**, 151 (1994).
6. Morterra, C., Verrato, G., Pinna, F., Signoretto, M., and Strukul, G., *J. Catal.* **149**, 181 (1994).
7. Yaluris, G., Larson, R. B., Kobe, J. M., Gonzalez, M. R., Fogash, K. B., and Dumesic, J. A., *J. Catal.* **158**, 336 (1996).
8. Farcasiu, D., Ghenciu, A., and Li, J. Q., *J. Catal.* **158**, 116 (1996).
9. Cheung, T. K., d'Itri, J. L., Lange, F. C., and Gates, B. C., *Catal. Lett.* **31**, 153 (1995).
10. Kustov, L. M., Kazansky, V. B., Figueras, F., and Tichit, D., *J. Catal.* **150**, 143 (1994).
11. Adeeva, V., de Haan, J. W., Janchen, J., Lei, G. D., Schunemann, V., van de Ven, L. J. M., Sachtler, W. M. H., and van Santen, R. A., *J. Catal.* **151**, 364 (1995).
12. Drago, R. S., and Kob, N., *J. Phys. Chem. B* **101**, 3360 (1997).
13. Fraenkel, D., *Chem. Lett.* 917 (1999).
14. Matsuhashi, H., and Arata, K., *Chem. Commun.* 387 (2000).
15. Olindo, R., Goeppert, A., Habermacher, D., Sommer, J., and Pinna, F., *J. Catal.* **197**, 344 (2001).
16. Hua, W. M., Goeppert, A., and Sommer, J., *J. Catal.* **197**, 406 (2001).
17. Xia, Y. D., Hua, W. M., Tang, Y., and Gao, Z., *Chem. Commun.* 1899 (1999).
18. Jin, T., Yamaguchi, T., and Tanabe, K., *J. Phys. Chem.* **90**, 4797 (1986).
19. Yadav, G. D., and Kirthivasan, N., *Chem. Commun.* 203 (1995).
20. Hino, M., and Arata, K., *Chem. Commun.* 1148 (1979); Hino, M., and Arata, K., *Chem. Commun.* 851 (1980).
21. Chen, F. R., Coudurier, G., Joly, J. F., and Vedrine, J. C., *J. Catal.* **143**, 616 (1993).
22. Lei, T., Xu, J. S., Tang, Y., Hua, W. M., and Gao, Z., *Appl. Catal. A Gen.* **192**, 181 (2000).
23. Biz, S., and Occelli, M. L., *Catal. Rev.—Sci. Eng.* **40**, 329 (1998).
24. Xia, Q. H., Hidajat, K., and Kawi, S., *Catal. Today* **68**, 255 (2001).
25. Anwander, R., Palm, C., Gerstberger, G., Groeger, O., and Engelhard, G., *Chem. Commun.* 1811 (1998).
26. Xia, Q. H., Hidajat, K., and Kawi, S., *Chem. Commun.* 2229 (2000).
27. McIntosh, D. J., and Kydd, R. A., *Microporous & Mesoporous Mater.* **37**, 281 (2000).
28. Ciesla, U., Fröba, M., Stucky, G., and Schüth, F., *Chem. Mater.* **11**, 227 (1999).
29. Gregerson, L. N., Siegel, J. S., and Baldridge, K. K., *J. Phys. Chem. A* **104**, 11,106 (2000).
30. Keller, A. A., Sandall, O. C., Rinker, R. G., Mitani, M. M., Bierwagen, B., and Snodgrass, M. J., *Ground Water Monit. Remediation* **20**, 114 (2000).
31. Kharoune, M., Pauss, A., and Lebeault, J. M., *Water Res.* **35**, 1665 (2001).
32. Amberg, A., Rosner, E., and Dekant, W., *Toxicol. Sci.* **61**, 62 (2001).
33. Bradley, P. M., Chapelle, F. H., and Landmeyer, J. E., *Appl. Environ. Microbiol.* **67**, 1975 (2001).
34. Marxsen, C. S., *Oil Gas J.* **99**, 20 (2001).
35. Erdal, S., and Goldstein, B. D., *Annu. Rev. Energy Environ.* **25**, 765 (2000).
36. Cooper, C., *Chem. Eng. News* **107**, 31 (2000).
37. Nadim, F., Zack, P., Hoag, G. E., and Liu, S. L., *Energy Policy* **29**, 1 (2001).
38. Horvath, T., Seiler, M., and Hunger, M., *Appl. Catal. A Gen.* **193**, 227 (2000).
39. Le Van, Mao, R., Le, T. S., Fairbairn, M., Muntasar, A., Xiao, S., and Denes, S., *Appl. Catal. A Gen.* **185**, 221 (1999).
40. Kim, J. S., Kim, J. M., Seo, G., Park, N. C., and Niiyama, S., *Appl. Catal.* **37**, 45 (1988).
41. Adams, J. M., Martin, K., McCabe, R. W., and Murray, S., *Clays Clay Miner.* **34**, 597 (1986).
42. Knifton, J. F., and Edwards, J. C., *Appl. Catal. A Gen.* **183**, 1 (1999).

43. Nikolopoulos, A. A., Kogelbauer, A., Goodwin, J. G., Jr., and Marcelin, G., *Catal. Lett.* **39**, 173 (1996).
44. Quiroga, M. E., Figoli, N. S., Sedran, U. A., *J. Chem. Eng.* **67**, 199 (1997).
45. Xia, Q. H., Hidajat, K., and Kawi, S., *Mater. Lett.* **42**, 102 (2000).
46. Xia, Q. H., Hidajat, K., and Kawi, S., *Stud. Surf. Sci. Catal.* **129**, 49 (2000).
47. Sing, K. S. W., Everett, D. H., Haul, R. A. W., Moscou, L., Pierotti, R. A., Rouquerol, J., and Siemieniewska, T., *Pure Appl. Chem.* **57**, 603 (1985).
48. Jentys, A., Pham, N. H., and Vinek, H., *J. Chem. Soc. Faraday Trans.* **92**, 3287 (1996).
49. Tatsumi, T., Koyano, K. A., Tanaka, Y., and Nakata, S., *J. Por. Mater.* **6**, 13 (1999).
50. White, R. L., Sikabwe, E. C., Coelho, M. A., and Resasco, D. F., *J. Catal.* **157**, 755 (1995).